Alt, J.C., Kinoshita, H., Stokking, L.B., and Michael, P.J. (Eds.), 1996
Proceedings of the Ocean Drilling Program, Scientific Results, Vol. 148

15. PALEOMAGNETIC AND ROCK MAGNETIC PROPERTIES OF HOLE 896A[1]

Simon Allerton,[2] Horst-Ulrich Worm,[3] and Laura B. Stokking[4]

ABSTRACT

Ocean Drilling Program Hole 896A was drilled 1 km southeast of the ODP deep-basement Hole 504B, 200 km south of the Costa Rica Rift. The magnetic properties (intensity of remanence, bulk susceptibility, inclination of stable remanence, and median destructive field) of 166 minicores from Hole 896A are presented. The basement in Hole 896A can be divided into three sections on the basis of its magnetic properties. The upper part, to 330 m below seafloor (mbsf), has relatively high intensity of remanence (J_0) and low susceptibility values. The middle section, between 330 and 360 mbsf, has high (J_0) and intermediate susceptibility values, and the lower section, below 360 mbsf, has low (J_0) and high susceptibility values. The magnetic mineralogy was investigated by monitoring the effect of heating on susceptibility. These results suggest that titanomaghemites occur throughout the hole and that titanomagnetites occur mainly below 330 mbsf. Some samples have evidence for minor amounts of hematite. The main cause of variation in the susceptibility and the median destructive field can be related to grain size. Grain size also controls J_0, although the degree of maghematization and the remanence mechanism of the magnetization also contribute. The magnetic properties of the upper part of Hole 896A, above the massive flow Unit 24, correlate with the upper part of Hole 504B above Unit 2D, at depths of 3796 and 3773 m below sea level, respectively. We suggest that the upper section corresponds to a late volcanic pile extruded onto a ponded flow that masks the earlier basement topography. This flow has probably acted as a major barrier to hydrothermal circulation. These results have significant implications for the interpretation of magnetic field data from ridges. The uppermost layer of late extrusive rocks has a high magnetization and a highly variable thickness, and may be an important contributor to variations in the magnetic signal at ridges.

INTRODUCTION

Our understanding of the magnetization of the oceanic crust comes largely from Deep Sea Drilling Project (DSDP) and Ocean Drilling Program (ODP) drilling (e.g., Furuta and Levi, 1983; Smith and Banerjee, 1986; Pariso and Johnson, 1991) and from ophiolites (e.g., Vine and Moores, 1972; Banerjee, 1980). Within these studies, ODP Hole 504B holds a special place as the deepest hole in ocean basement, penetrating 1.8 km of oceanic basement, including more than 1 km of sheeted dikes. These studies, particularly those of DSDP/ODP drill holes, by their nature lead to a one-dimensional layered model of the magnetic properties of the oceanic crust. ODP Hole 896A was drilled 1 km southeast of Hole 504B and provides an opportunity to test the validity of these layered models. In this chapter, we describe the rock magnetic properties of Hole 896A, discuss their origin, and compare them with those of DSDP/ODP Hole 504B.

GEOLOGICAL SETTING AND DRILLING OF HOLE 896A

Hole 896A is located at 1°13.006′N, 83°43.392′W, about 1 km southeast of Hole 504B (Fig. 1) and about 200 km south of the spreading axis of the Costa Rica Rift (Alt, Kinoshita, Stokking, et al., 1993). It was drilled on a bathymetric high over a basement high observed on single-channel seismic reflection data, in a water depth of 3448 m below sea level (mbsl). Basement was reached at 179 m below seafloor (mbsf) and was cored from 195 to 469 mbsf (274 m), with a recovery of about 74 m of rock. Basement is composed of extrusive and shallow intrusive lithologies including pillow lavas (57%), massive units (38%), breccias (5%), and two small dikes. The volcanic section can be divided into upper and lower sections. The upper section (195–390 mbsf) is dominantly plagioclase-olivine phyric, and the lower section (390–469 mbsf) is commonly plagioclase-olivine-clinopyroxene phyric.

The ages of Sites 896 and 504 have been determined from their position relative to the magnetic anomaly time scale. Hobart et al. (1985) identified Site 504 as 70% across the 5.62–6.06-Ma reversal, according to the LaBrecque et al. (1977) time scale, which corresponds to an age of 5.93 Ma. Site 896 lies at a position 85% across this reversal, giving an age of 5.99 Ma. Updated time scales (e.g., Cande and Kent, 1992) now place this reversed period in the interval 6.376–6.744 Ma, yielding revised ages of 6.63 Ma for Site 504 and 6.68 Ma for Site 896. The Costa Rica Rift has an intermediate spreading rate (3.6 cm/yr half-rate) and a relatively simple crustal structure with a half-graben tilted away from the ridge, as imaged on single-channel seismic reflection profiles (Langseth et al., 1988).

MEASUREMENT OF MAGNETIC PROPERTIES

This study is based on measurements from 71 shipboard samples and from shore-based studies of 66 samples in Oxford, United Kingdom, samples) and 29 samples at BGR, Grubenhagen, Germany. Of these 166 samples, 87 (52%) are from pillow flows, 77 (47%) are from massive flows, and 2 (1%) are from breccias. The sample set thus slightly underrepresents the pillow flows and breccias and overrepresents the massive flows in the recovered core. As recovery is only about 27%, the actual proportions of these lithologies in the drilled section may be significantly different. Because pillows and breccias tend to break up during drilling, these lithologies are probably significantly underrepresented in the core and in this study.

Properties measured include the measurement of the direction and intensity of natural remanence, bulk susceptibility, acquisition of isothermal remanent magnetization (IRM), and variation of susceptibility with temperature (Table 1). The intensity of remanence and the volume susceptibility are calculated using volumes derived using

[1]Alt, J.C., Kinoshita, H., Stokking, L.B., and Michael, P.J. (Eds.), 1996. *Proc. ODP, Sci. Results*, 148: College Station, TX (Ocean Drilling Program).

[2]Department of Geology and Geophysics, University of Edinburgh, The Grant Institute, West Mains Road, Edinburgh EH9 3JW, United Kingdom. simona@glg.ed.ac.uk

[3]Bundesanstalt für Geowissenschaften und Rohstoffe, Stilleweg 2, Postfach 510153, D-30631 Hannover, Federal Republic of Germany.

[4]Ocean Drilling Program, Texas A&M University Research Park, 1000 Discovery Drive, College Station, TX 77845-9547, U.S.A. stokking@cook.tamu.edu

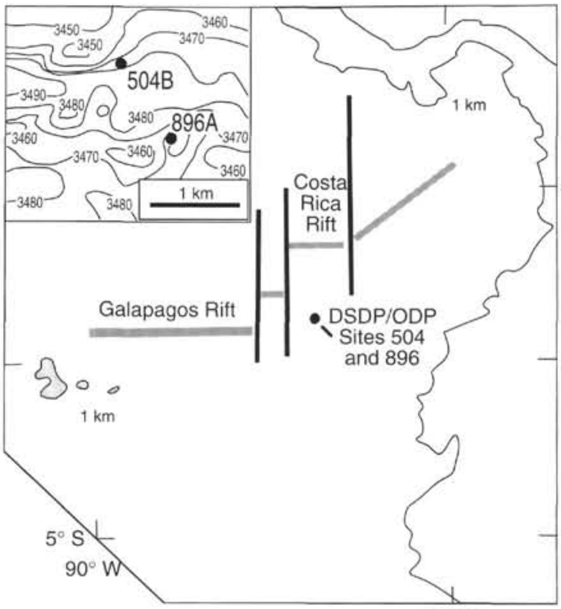

Figure 1. Location of DSDP/ODP Sites 504 and 896 south of the Costa Rica Rift in the eastern equatorial Pacific (modified from Hobart et al., 1985). Bathymetric contours in kilometers. Inset: Detailed bathymetry (in meters) at Hole 504B and 896A.

either Archimedes' principle (shipboard samples) or a simple geometrical estimate (Oxford and BGR).

The magnetic properties reported here are essentially similar to those described in Alt, Kinoshita, Stokking, et al. (1993), but are based on a larger sample set. Because the cores are free to rotate in the barrel, the declinations are measured relative to an arbitrary "working" reference frame, rather than to an in situ reference, so only the inclination can be obtained from these partially oriented samples.

The various magnetic properties discussed in detail below show a variation with depth. Significant changes are noted at about 330 mbsf (top of Unit 24) and at 360 mbsf (top of Unit 31). These breaks correspond to the tops of massive flow units.

MAGNETIC REMANENCE

Magnetic remanence was measured on board ship using a 2G cryogenic magnetometer, in Oxford using either a CCL cryogenic magnetometer or a Molspin spinner magnetometer, and at BGR using a 2G cryogenic magnetometer. General procedure involved stepwise alternating field (AF) demagnetization up to fields of 100 mT. Stable remanence directions were defined using a least-squares algorithm (Kirschvink, 1980).

Above about 360 mbsf, the majority of samples show a stable single component on AF demagnetization, with a high degree of linearity on vector end-point diagrams and clustered directions in stereographic projection (Fig. 2A). They generally have some low-coercivity magnetization, which is generally randomly oriented and can be removed by 10 mT of AF treatment. This contrasts with other drilling-induced remanences (e.g., Allerton et al., 1995), which typically have consistent, steep inclinations. In this upper part of the hole, the inclinations of the high-coercivity component are generally close to horizontal (mean inclination = $-7.5° \pm 10.2°$, compared with an expected paleoinclination = $-7°$).

In this upper part of the hole there is a suggestion that the inclinations vary in a systematic, cyclical manner, with an amplitude of about 10° and a wavelength of about 70 m (Fig. 3A, B). This behavior may reflect secular variation of the sequence, suggesting that eruption was relatively continuous, at a rate of about 150 m in a few thousand years. Some individual samples have anomalous inclinations (Samples 148-896A-7R-1, 12–14 cm; 8R-1, 29–31 cm; 8R-1, 95–97 cm; and 12R-2, 23–25 cm), and yet all the other characteristics of the magnetization are similar to the rest of the sequence. It is most likely that these are from pillow lavas that were moved after they had acquired their magnetization.

Below 360 mbsf, the AF demagnetization produces a less clearly linear magnetization, shown by a large maximum angular deviation (MAD) of 4°, compared to a MAD of 2° in the upper section. On a stereographic projection, the majority of samples from below 360 mbsf plot as a segment of a great circle or as highly scattered paths, which indicates the presence of multiple components with overlapping coercivity spectra (Fig. 2B). In this part of the hole, inclinations are very scattered even from the same lithologic unit (cf., e.g., results from Unit 37; Table 1). We do not consider that the directions from this lower interval represent any consistently meaningful measurement of the paleomagnetic field.

Samples from massive flow Units 31–36 and 49 and pillow Unit 47 commonly carry a high-coercivity component that is not removed during AF demagnetization. Hematite reported in some thin sections from the massive Units 31–36 may be the carrier of this high-coercivity magnetization.

Although we cannot compare full directional data (declination and inclination) from the core as a whole, it is possible to compare directional data from individual core pieces for the few cases where more than one sample for each piece of core has been measured. Of the 37 pairs of samples, 22 are separated by 10° or less, and 28 are separated by 20° or less. This compares with the stable inclinations for the same samples from the same pieces, for which 36 pairs are separated by less than 10° of inclination, and one pair is separated by 33° of inclination. The significantly larger scatter for the full directional data at least partly results from the inclusion of pieces with multiple subpieces—that is, broken pieces of core that can be fitted together. The larger values (>21°) are all from such pieces, except for Samples 148-896A-17R-2, 28–30 cm, and 17R-2, 38–40 cm, which suggests that these pieces were poorly matched before the cores were sliced. Unfortunately, in the section below 360 mbsf, where the fidelity of the magnetic signal is in doubt, only two pieces with two samples per piece were sampled. One of these pairs gives an inclination difference of 33°; the other pair gives an inclination difference of 3°.

The absence of the drilling-induced remanence so often reported for ODP cores (e.g., Ade-Hall and Johnson, 1976; Johnson, 1978; Lowrie and Kent, 1978) makes it possible to use the initial intensity of the sample (J_0) as a direct measure of the in situ remanence. There is no need to apply a correction such as those described for other studies of the magnetism of the ocean basement (e.g., Pariso and Johnson, 1991). Plotting the intensity against depth below basement (Fig. 3C) shows a small change below 330 mbsf and a more significant change beneath 360 mbsf (see Table 2).

The stability of magnetic remanence is indicated by the median destructive field (MDF, the AF required to demagnetize the sample to one-half its initial intensity). Plotted against depth (Fig. 3D), this property also shows a distinct reduction below 330 mbsf and no significant change below 360 mbsf (see Table 2).

INDUCED MAGNETIZATION

The magnetic susceptibility of the samples is dependent on the composition, concentration, and grain size of the magnetic minerals in the rock. Although paramagnetic minerals, such as amphiboles and pyroxenes, make some contribution, the susceptibility in these rocks is dominated by the effects of ferro- and ferrimagnetic minerals. The

Table 1. Paleomagnetic and rock magnetic measurements of samples from Hole 896A.

Core, section, interval (cm)	Piece	Lithology	Unit	Depth (mbsf)	Bulk susceptibility ($\times 10^{-3}$ SI units)	J_0 (A/m)	Relative declination (°)	Inclination (°)	Maximum angular deviation (°)	Median destructive field (mT)	J_{rs} (A/m)	H_{sat} (T)
148-896A-												
1R-1, 47	11	P	3	195.6	8.6	12.4	299	–2		50		
1R-1, 87	18	P	3	196.0	12.5	16.2	268	–12		28	220.1	0.11
2R-1, 3	1	M	4	201.1	14.3	7.0	69		1.0	10		
2R-1, 82	19	M	7	201.7	13.4					15	178.8	0.15
3R-1, 19	4	P	8	210.1	2.0	4.8	90	–19	2.0	37		
3R-1, 38	7	P	8	210.3	3.7	10.3	67	–10				
3R-1, 45	7	P	8	210.4	4.1	9.6	67	–8	2.0	25		
3R-1, 63	8	P	8	210.5	4.6	11.5	289	–7	4.0	27		
3R-1, 68	8	P	8	210.6	9.4	9.3	284	–7	1.0	17		
3R-1, 78	9	M	9	210.7	10.2	8.6	118	–9		18	203.5	0.14
3R-1, 96	9	M	9	210.9	12.5		282	–5	1.0			
4R-1, 44	9a	P	9	219.3	12.1	11.5	110	–8		24	206.3	0.14
4R-1, 49	9a	P	9	219.4	10.0	7.6	105	–12				
4R-1, 68	9c	P	9	219.6	13.2	20.7	139	–8		25		
5R-2, 27	1c	P	10	230.2	7.4	13.1	192	–13	1.6	26		
5R-2, 38	1d	P	10	229.7	3.2	8.3	233	–14		50		
5R-2, 125	13	P	10	231.2	6.6	11.5	276	–4	2.9	26		
5R-2, 126	13	P	10	230.6	5.2		280	–3	3.0			
5R-3, 43	5b	M	11	231.2	10.9	3.7	334	–13		17	189.9	0.17
5R-3, 62	8	M	11	231.4	11.7	15.2	235	–9		15	292.2	0.16
6R-1, 39	5a	P	12	238.3	6.6		92	–13	3.0			
6R-1, 48	5b	P	12	238.4	7.9	13.2	75	–5	1.2	26		
6R-1, 52	5c	P	12	238.4	6.1	16.0	83	–15		62		
6R-1, 93	9b	P	12	238.8	17.4	22.5	344	–19	1.0	15		
6R-2, 3	1a	P	12	239.4	1.4	3.1	56	–17		60	51.2	0.29
6R-2, 11	1b	P	12	239.5	0.9	1.9	279	–15	3.0	44		
6R-2, 89	10a	P	12	240.3	4.5	12.3	43	–10		40		
6R-3, 8	1	P	12	240.9	7.4	15.9	255	–16		30	245.5	0.15
7R-1, 12	3	P	13	247.5	1.2	1.0	35	31	1.3	30		
7R-1, 38	7	P	13	247.8	2.2	3.5	312	0	2.0	40		
7R-1, 58	10	P	13	248.0	5.0	12.0	222	–12		34	228.6	0.17
7R-1, 78	13	P	14	248.2	6.8	12.4	87	–9	0.0			
7R-1, 80	13	P	14	248.2	10.3	15.2	88	–10		17	268.7	0.13
7R-1, 101	15	P	14	248.4	6.8	12.7	215	–11				
8R-1, 29	7	P	14	257.4	9.1	11.4	183	–34			251.2	0.10
8R-1, 95	19	P	14	258.1	4.5	8.8	39	–60	3.8	28		
9R-1, 32	6	P	14	267.0	11.8	9.7	86	19	1.2			
9R-1, 42	7	P	14	267.1	5.2	11.1	251	–1	2.0	28		
9R-1, 135	25	P	14	268.1	7.4	7.3	72	–11	2.0	18		
9R-1, 138	25	P	14	268.1	11.9	10.9	71	–6		20	244.0	0.12
9R-2, 4	1	P	14	268.2	5.0	14.8	211	–7		45	272.3	0.15
9R-2, 6	1	P	14	268.2	5.6	10.6	210	–7	1.0	28		
9R-2, 44	4	P	14	268.5	7.2	10.8	236	–3	3.0	23		
10R-1, 70	8b	M	14	277.1	5.6	12.4	220	–3		25		
10R-1, 80	8d	M	14	277.2	10.4	12.3	33	–11				
10R-1, 85	8e	M	14	277.3	9.7	15.6	51	–2		27	265.0	0.11
10R-1, 104	9b	M	14	277.4	6.8	16.6	90	–1	2.0	19		
10R-1, 116	9c	M	14	277.6	8.1	15.3	16	–1		34	265.8	0.14
11R-1, 32	3d	P	14	286.3	11.2	9.8	19	–5		17	216.5	0.08
11R-1, 37	3e	P	14	286.4	10.3	7.5	16	–3				
11R-1, 51	3e	P	14	286.5	13.5	10.7	13	–9	0.3	13		
11R-1, 120	10c	P	14	287.2	5.6	9.2	126	–12	3.0	34		
11R-3, 19	4	M	15	289.1	13.4	16.0	56	–7	1.0	20		
11R-3, 90	15	P	14	289.9	11.8	18.7	305	–8	1.7	17		
12R-1, 20	3b	P	16	295.3	11.7	10.2	41	–13				
12R-1, 53	8	M	16	296.1	14.4	11.3	337	–12	0.8			
12R-1, 63	9c	M	16	295.7	13.4		223	–8	1.0			
12R-1, 68	9c	M	16	296.3	13.6	15.3	222	–8		15	264.2	0.14
12R-1, 78	10b	M	16	296.4	13.5	13.6	110	–12		16	249.2	0.12
12R-1, 80	10b	M	16	296.4	12.8	13.6	102	–21		16		
12R-1, 82	10b	M	16	295.9	11.1	9.7	104	–16	2.0	15		
12R-1, 141	18b	M	16	296.5	9.4	5.8	295	–11	2.0	20		
12R-2, 9	1b	M	17	297.1	17.8		262	–12			286.4	0.40
12R-2, 23	2	M	17	297.2	13.8	8.6	42	17	1.0			
14R-2, 28	3	P	19	316.3	6.7	14.1	25	–14		31	239.6	0.15
14R-2, 113	16a	M	21	317.1	17.0	11.9	91	–8		13	216.7	0.09
14R-2, 118	16b	M	21	317.2	16.1	6.2	93	–4	2.0			
14R-3, 16	3	M	21	317.7	8.1	10.8	56	–6				
14R-3, 65	11	M	21	318.2	10.4		14	–11	1.0			
15R-1, 3	1	M	22	324.3	0.0	10.6	326	–21	1.0	12		
15R-1, 103	15	P	23	325.3	8.9	16.2	24	–12		33	294.5	0.13
15R-1, 105	15	P	23	325.4	7.6	11.1	13	–10	1.0			
15R-1, 128	18a	P	23	325.6	7.8	13.3	168	–13	1.3	28		
15R-2, 73	7b	P	23	326.4	12.9	9.8	72	–9	1.0	16		
15R-2, 123	16	P	23	326.9	9.7	5.8	150	–9	2.0	21		
16R-1, 21	3b	P	24	334.1	16.9	13.2	54	–6		17		
16R-1, 32	3b	P	24	334.2	18.1	9.4	56	–8		17	253	0.09
16R-1, 66	8	M	24	334.6	22.0	11.2	69	–10				
16R-1, 124	9d	M	24	335.1	19.6	3.2	230	–5	2.0	9		
16R-2, 11	1a	M	24	335.3	24.5	4.3	334	–8				
16R-2, 14	1b	M	24	335.3	23.2	4.3	326	–2	0.0	7		
16R-2, 27	1c	M	24	335.7	24.2	4.4	330	–6	0.6	5		
16R-2, 34	1c	M	24	335.6	34.4	5.0	339	–6		8	179.3	0.11
16R-2, 50	1e	M	24	335.7	26.6	5.8	216	14	2.0	9		
16R-2, 55	1e	M	24	335.8	21.1	2.4	217	10	2.0	13		

Table 1 (continued).

Core, section, interval (cm)	Piece	Lithology	Unit	Depth (mbsf)	Bulk susceptibility ($\times 10^{-3}$ SI units)	J_0 (A/m)	Relative declination (°)	Inclination (°)	Maximum angular deviation (°)	Median destructive field (mT)	J_{rs} (A/m)	H_{sat} (T)
148-896A-												
16R-2, 113	4b	M	24	336.3	17.3	6.6	276	−5	2.0	7		
16R-2, 130	4c	M	24	336.6	20.4	7.9	284	−14		10		
16R-2, 132	4c	M	24	336.6	19.3	7.4	279	−6		10	223.3	0.58
16R-3, 55	1d	M	24	337.3	18.1	2.0	279	−13	2.0	8		
16R-3, 81	4a	M	24	337.5	19.6	4.5	90	−9	3.0	8		
16R-3, 85	4b	M	24	337.5	0.0	4.2	110	−12	2.1	7		
16R-3, 88	4b	M	24	337.6	23.0	4.4	111	−3		9	211.0	0.25
17R-1, 1	1a	P	25	343.5	19.3	14.4	344	15		17	273.0	0.09
17R-1, 82	10b	P	26	344.3	20.2	4.8	206	−10		16	213.7	0.10
17R-1, 85	10b	P	26	344.4	16.7	3.7	204	−2				
17R-1, 136	16a	P	27	344.9	23.5	6.6	285	−8	0.8	10		
17R-1, 139	16b	P	27	344.9	22.2	7.2	280	−7	1.0	9		
17R-2, 19	3a	P	27	345.2	21.1	8.1	148	−10	0.9	13		
17R-2, 40	3e	P	27	345.4	24.2	4.7	317	−6	2.0	10		
17R-2, 126	11	P	27	346.3	23.5	16.8	44	−6		13	287.1	0.16
17R-2, 140	12b	P	27	346.4	22.2	7.3	193	0	1.0	9		
17R-3, 37	4a	P	27	346.8	22.5	15.6	65	−3	2.0	13		
17R-3, 57	4a	P	27	347.0	21.8	9.6	57	−9	2.0	4	320.4	0.08
17R-3, 86	8	P	28	347.3	16.9	10.2	215	−6	2.0	10		
17R-3, 89	8	P	28	347.3	22.4	9.7	217	−7		14	233.9	0.08
17R-4, 28	2d	P	28	348.2	23.5	12.1	239	−2		12	240.6	0.20
17R-4, 36	2d	P	28	348.3	22.7	8.1	275	−2	1.0	9		
17R-4, 97	9	M	28	348.9	27.3	8.4	149	3				
17R-4, 99	9	M	28	348.9	30.3	15.5	149	2		8		
17R-5, 21	4	M	28	349.6	23.8	1.7	133	−7	0.5	10		
18R-1, 72	6b	P	29	353.8	20.1	13.5	230	11		17		
18R-1, 102	9b	P	29	354.1	21.0	13.8	166	0		17	275.9	0.08
18R-1, 127	11b	P	29	354.4	24.4	6.2	250	14	1.3	18		
18R-2, 60	10	P	30	355.2	8.8	8.3	322	−28		24		
19R-1, 23	5a	P	30	356.2	25.8	13.6	115	−26		19	456.4	0.95
20R-1, 63	15	M	31	364.1	36.5	10.4	267	−52		18		
20R-1, 108	22	M	31	364.5	47.0	4.4	288	−6		9		
21R-1, 58	10	M	31	373.6	30.0	1.4	338	−16		17		
21R-1, 105	17	M	31	374.1	20.1	1.4	355	−11				
21R-1, 137	20	M	31	374.4	19.6	1.0	130	−5	2.0	8	202.5	0.05
21R-2, 10	2	M	31	376.1	20.1	1.4	137	−6				
21R-2, 85	9b	M	31	375.3	47.0	2.4	139	13		3		
21R-2, 118	11b	M	32	375.7	23.5	6.7	52	−35	0.6	9		
21R-2, 133	13a	M	32	375.8	31.0	3.8	58	−59		10		
22R-1, 45	5b	M	32	383.1	20.8	6.6	184	−37	1.0	14		
22R-1, 107	13	M	32	383.7	36.1	13.0	233	−31		21		
22R-3, 11	2	M	33	385.7	29.5	3.8	116	−37		9		
22R-3, 26	3	M	33	385.9	50.7	5.0	84	−44		10		
22R-4, 9	1b	M	33	388.0	25.2	4.5	284	−38	1.3	11		
23R-1, 18	2	B	35	392.3	36.8	1.0	185	52		4		
23R-1, 77	11	M	36	392.9	26.5	4.6	67	−7		18		
23R-2, 20	2a	M	36	393.8	19.6	1.4	97	−12	2.0	8		
23R-2, 48	4	M	36	394.1	22.0	1.3	75	−7	3.0	7		
23R-2, 82	7	M	36	394.4	18.6	0.8	173	−20	3.0	10	197.5	0.05
23R-3, 6	1	M	36	395.1	37.7	2.5	43	43		5		
23R-3, 132	17	M	36	396.3	40.1	3.3	187	48		5	159.2	0.13
24R-1, 16	1	M	36	402.0	20.2	2.3	224	66	6.4	3		
24R-1, 61	4	M	36	402.4	23.4	0.5	350	0	7.0	8		
24R-1, 122	8	M	36	403.0	18.7	2.4	158	55	6.3	5		
24R-1, 125	8	M	36	403.1	45.3	4.1	172	22		5		
24R-2, 85	10	M	36	404.2	23.0	1.2	272	44	3.0	13		
24R-2, 114	13	M	36	404.4	24.2	1.3	345	27	3.0	8	195.6	0.05
24R-3, 52	5	M	36	405.3	23.3	0.5	144	32	4.7	6		
24R-3, 140	14b	M	36	406.2	44.7	2.9	214	41		2		
24R-4, 53	7	M	36	406.7	24.3	1.3	242	24	2.0	7		
24R-5, 90	9	M	36	408.6	25.1	1.6	35	−30	3.0	4	171.2	0.05
24R-5, 118	12	M	36	375.7	23.5	1.7	154	−36	5.6	5		
25R-1, 34	6	P	37	411.6	13.7	2.7	287	15	5.0	15	257.4	0.07
25R-1, 49	6b	P	37	411.8	20.3	4.5	310	12		20		
25R-1, 141	17	P	37	412.7	14.6	2.0	144	32	2.0	10		
25R-2, 89	16	P	37	413.7	11.2	2.4	28	−31	3.0	15	244.9	0.08
25R-3, 52	7	P	37	414.7	19.2	3.6	335	2		17		
26R-1, 63	9b	M	38	421.6	16.6	3.4	95	10		9		
26R-1, 118	17	P	40	423.7	23.2	2.1	7	24	3.3	5		
26R-2, 27	4	P	41	422.8	18.2	4.5	97	16		18		
26R-3, 19	1c	P	42	433.7	17.1	2.2	284	17	1.9	17		
27R-1, 18	1b	P	42	430.7	13.8	1.8	200	53				
27R-1, 69	8	P	43	431.2	41.0	2.8	124	−2		9		
27R-3, 43	5	P	47	433.8	17.1	2.3	300	−8	6.0	14	294.3	0.07
28R-1, 120	18	P	47	441.2	14.9	2.4	136	20	2.2	21		
28R-2, 15	1b	P	47	441.6	25.1	3.3	94	22		19		
28R-2, 39	3b	P	47	441.8	29.0	8.2	273	19		16		
29R-1, 93	13	M	49	450.6	63.2	4.4	266	69		4		
29R-2, 7	1c	P	50	451.2	22.4	0.6	4	−13	11.0	9		
30R-1, 36	6	B	50	459.7	24.5	3.7	226	−41		20		
30R-1, 98	12b	P	50	460.3	29.4	0.5	277	−50	3.5	14		

Notes: Lithology: P = pillow, M = massive, and B = breccia. The declination is measured relative to the arbitrary cut face of the core. The dashed lines mark the intervals discussed in the text.

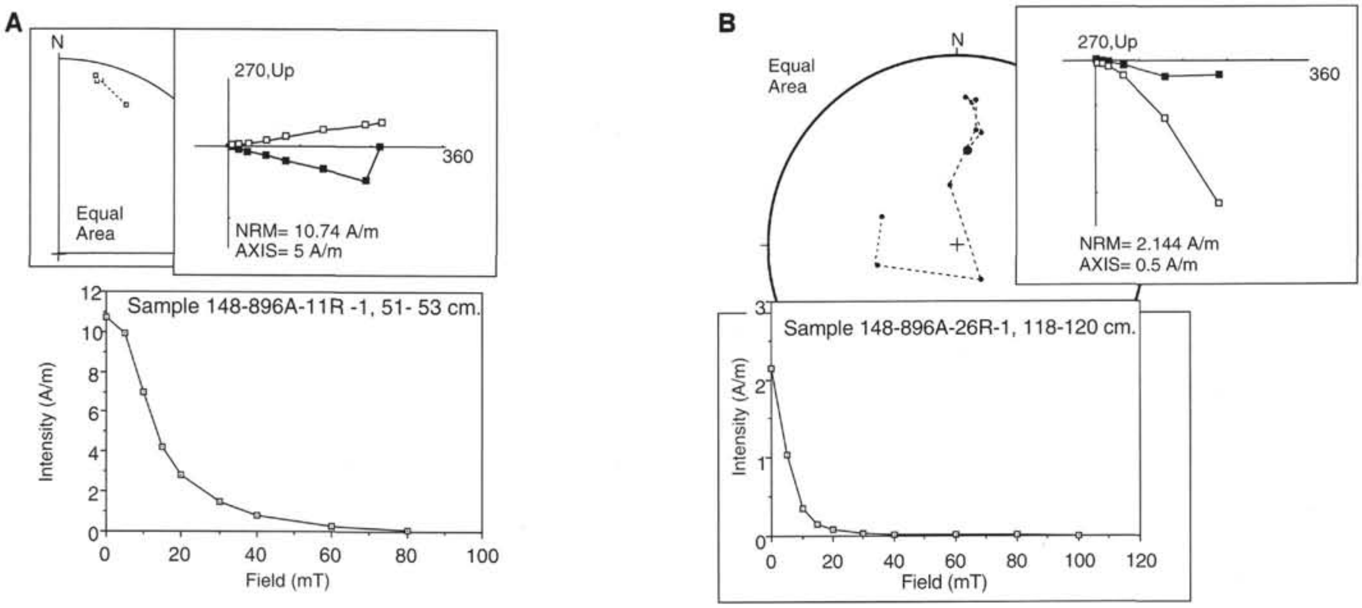

Figure 2. Alternating field demagnetization behavior. Orthogonal vector diagrams (solid squares are horizontal projections, open squares are vertical projections), stereographic projections, and intensity vs. demagnetizing field. **A.** Note the clear linearity during demagnetization and the tight grouping in stereographic projection. **B.** Sample 148-896A-26R-1, 118–120 cm. Note that the data plot as a segment of a great circle, and they do not plot as a linear segment on the orthogonal vector diagram.

bulk susceptibility was measured using a Geofyzika Brno Kappabridge, both aboard ship and in Oxford. The mean susceptibility is $17.6 \pm 10.6 \times 10^{-3}$ SI units. The susceptibility increases below 330 mbsf, and again below 360 mbsf, with an increase in variability (Fig. 3E; Table 2).

ISOTHERMAL REMANENT MAGNETIZATION

The acquisition of isothermal remanent magnetization was investigated on board using an ASC impulse magnetizer. Further measurements were concluded in Oxford using a Molspin pulse magnetizer. The majority of samples exhibited a steep gradient of IRM acquisition up to the saturation level (H_{sat}, defined as 95% of the maximum IRM intensity), after which no significant increase in intensity was noted with increasing applied field. Saturation of the samples in fields between 70 and 200 mT indicates the predominance of (titano)magnetite and/or (titano)maghemite. The saturation of a few samples, mostly from massive flows, in fields greater than 200 mT suggests the presence of additional, high-coercivity phases. Some anomalously high values (Samples 148-896A-16R-2, 132–134 cm, and 148-896A-19R-1, 23–25 cm) may be associated with the occurrence of secondary hematite. There is some suggestion of a decrease in H_{sat} at about 350 mbsf. The saturation remanence, J_{rs}, has a mean value of 239 ± 58 A/m.

HIGH-TEMPERATURE SUSCEPTIBILITY

The variation of magnetic susceptibility with temperature was studied to determine the mineralogy of the magnetic phases present in the samples. The procedure is similar to measurements of saturation remanence with temperature, but can give additional information about domain states. Low-field susceptibility was monitored during both heating and cooling cycles, up to a maximum temperature of 700°C using a CS2 attachment to a Geofyzika Brno Kappabridge. Powdered samples were measured in air, which may have enhanced the degree of oxidation in the measurements. This probably has the greatest effect on the cooling curves, after the samples had been heated to 700°C. The system is particularly useful for distinguishing between titanomagnetites and titanomaghemites. Problems occur in the interpretation of phases with high Curie temperatures, as it is difficult to separate original phases from the products of alteration. Hematite, for example, indicated by susceptibilities between 600° and 700°C, may result either from in situ hydrothermal alteration or by breakdown of titanomaghemites. It is commonly difficult to identify Curie temperatures by taking the gradient of the slope, particularly for the first peak, because of the corruption of the slope introduced by the overlap of old phases and the formation of new phases makes the errors introduced by fitting a gradient unacceptable. Instead, we identified the peak temperature corresponding to each phase.

The temperature dependence of susceptibility of 23 samples was measured. On the basis of their high-temperature behavior, the samples can be separated into two different types.

Type I is irreversible, with the heating curve exhibiting either two peaks separated by a trough or two steep segments separated by a shallower segment. These curves are similar to saturation magnetization vs. temperature for extrusive rocks from Hole 504B (e.g., Pechersky et al., 1983; Furuta, 1983; Donovan and O'Reilly, 1983), which have been interpreted as titanomaghemites that invert to a multiphase product on heating. The thermomagnetic curves are reversible up to the first peak (typically close to 300°C), but then exhibit irreversible behavior, and the characteristic "inversion" is in the range of 350°–470°C and peaks between 400° and 520°C (see Table 3).

The cooling curves for the type I irreversible curves yield information on the complex products of inversion and subsequent oxidation. In some cases, the cooling curve has a gradual slope that peaks at about 200°C (type Ia; Fig. 4A, B). These probably represent inversion of the titanomaghemite to a titanomagnetite with a similar Fe/Ti ratio. These curves are reversible on further heating and cooling. Some curves have a high-temperature peak (between 500° and 600°C) on cooling (type Ib; Fig. 4C), which may correspond to a magnetite or Ti-depleted titanomagnetite resulting from exsolution during inversion. The third type of irreversible curve involves a high-temperature phase (600°–700°C) on cooling (type Ic, Fig. 4D), which

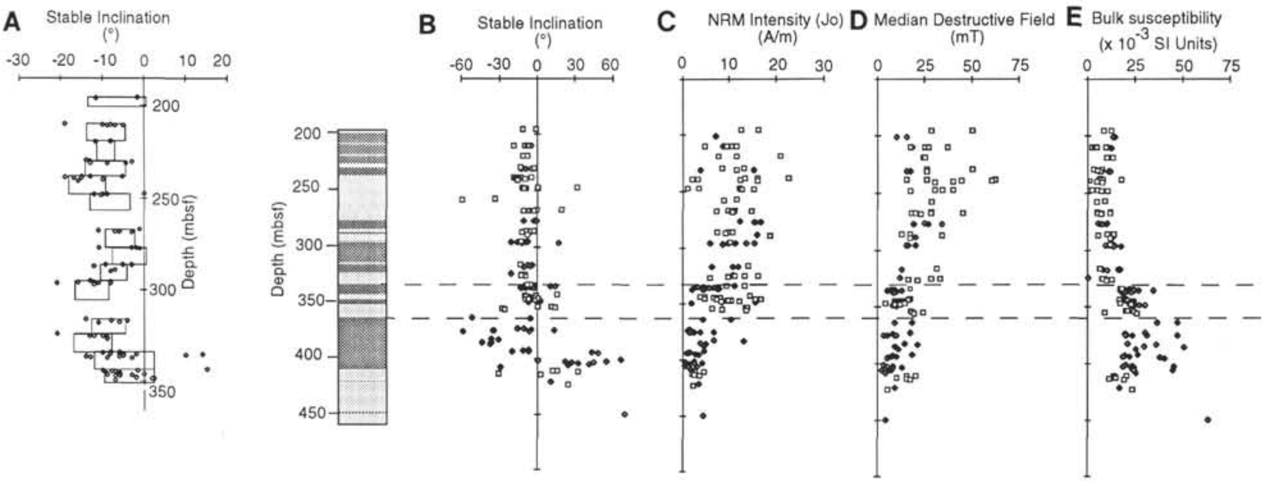

Figure 3. **A–E.** Magnetic properties vs. depth. Samples from massive flows are displayed as diamonds, and samples from pillow flows are squares. The lithostratigraphy is also marked schematically: light shaded areas are pillow flows and dark shaded areas are massive flows. In the inclination of the upper part of the hole (Fig. 3A), the boxes represent mean inclinations for individual cores and the depth over which the core was taken. Samples with an inclination that deviates significantly from the main group, as discussed in the text, have been omitted.

Table 2. Mean paleomagnetic and rock magnetic measurements from Hole 896A and upper part of Hole 504B (from the top of basement to 830 mbsf).

Depth (mbsf)	Lithology	Bulk suceptibility (× 10^{-3} SI units)	NRM intensity (J_0) (A/m)	Stable inclination (°)	Median destructive field (mT)	Samples (N)
Hole 896A:						
195<	All	17.6 ± 10.6	7.8 ± 5.1	−4.3 ± 20.8	17.1 ± 11.2	166
<460	Massive	22.3 ± 11.2	6.3 ± 6.3	−3.5 ± 24.4	11.2 ± 6.2	77
	Pillow	0.0 ± 0.0	0.0 ± 0.0	0.0 ± 0.0	0.0 ± 0.0	0
	Breccia	30.7 ± 8.7	2.4 ± 1.9	5.5 ± 65.8	12.0 ± 11.3	2
195<	All	9.1 ± 4.0	11.2 ± 4.2	−9.2 ± 10.5	26.2 ± 11.8	75
<330	Massive	11.9 ± 3.0	11.4 ± 3.7	−8.1 ± 7.6	18.1 ± 5.9	26
	Pillow	0.0 ± 0.0	0.0 ± 0.0	0.0 ± 0.0	0.0 ± 0.0	0
330<	All	21.9 ± 4.2	8.0 ± 4.1	−4.6 ± 8.9	11.6 ± 4.5	40
<360	Massive	23.2 ± 4.5	5.7 ± 3.4	−4.3 ± 7.5	8.5 ± 1.8	18
	Pillow	0.0 ± 0.0	0.0 ± 0.0	0.0 ± 0.0	0.0 ± 0.0	0
360<	All	26.8 ± 11.0	3.1 ± 2.4	2.8 ± 33.1	10.7 ± 5.6	51
<460	Massive	29.6 ± 11.5	3.2 ± 2.8	0.2 ± 35.7	8.7 ± 4.8	33
	Pillow	0.0 ± 0.0	0.0 ± 0.0	0.0 ± 0.0	0.0 ± 0.0	0
	Breccia	30.7 ± 8.7	2.4 ± 1.9	5.5 ± 65.8	12.0 ± 11.3	2
Hole 504B:		26.2 ± 13.8	6.2 ± 5.5	−22.4 ± 20.4	13.5 ± 7.5	
Above Unit 2D	11.7 ± 5.8	11.2 ± 5.0	−10.8 ± 6.0	25.4 ± 13.7		
Unit 2D and below	27.7 ± 13.5	5.7 ± 5.3	−23.7 ± 21.0	12.3 ± 5.5		

Note: Errors are given as 1 standard deviation. N = number of samples.

probably indicates that hematite is a product of inversion. Type I behavior was observed throughout the hole, in both massive and pillow lithologies.

Type II curves are nearly reversible in shape, though not in magnitude, with a single peak matched by a similar cooling curve (Fig. 4E). These curves can be interpreted as an indication of the presence of titanomagnetite. The majority of the rype II curves occur in samples taken from below 330 mbsf (above 330 mbsf, only Sample 148-896A-3R-1, 68–71 cm, shows type II behavior), in both pillow and massive flows.

Almost all the samples, of both types, show a bulge on the heating curve, also commonly seen on the cooling curve, in the interval between 50° and 200°C. The apparent reversibility of this section is characteristic of a mineral that is chemically stable up to 700°C, and may represent a component of original titanomagnetite. The Curie temperature of titanomagnetites is highly dependent on the composition, particularly of cations such as aluminum or magnesium replacing titanium (O'Reilly, 1984). Previous studies of the oxide compositions of the extrusive rocks from DSDP Hole 504B (Donovan and O'Reilly, 1983) have determined x values of about 0.6 for titanomagnetites with a general formula of $Fe_{3\text{-}d\text{-}x}\,M_d\,Ti_x\,O_4$, where M = Al, Mg, Mn, and Cr. The minor cations, principally Al, have d values of about 1.6, sufficient to significantly effect the Curie temperature (Ozdemir and O'Reilly, 1981). Despite this, the temperature interval of the bulge between 50° and 200°C is consistent with a stoichiometric titanomagnetite with $x = 0.6$ ($T_c = 150$°C). This phase may thus represent a small component of unoxidized original titanomagnetite.

For most samples, the heating curve shows little susceptibility above 600°C, although some of these samples show a gradual rise in susceptibility on the cooling sample between 700° and 600°C, which is characteristic of hematite generated during heating. Genuinely reversible behavior in the 600°–700°C interval was identified only in three samples (see Table 3).

The following conclusions can be drawn from the thermomagnetic behavior: the majority of samples show evidence of the typical thermomagnetic behavior ascribed to titanomaghemite and inversion to multiphase products (e.g., Donovan and O'Reilly, 1983). Some samples show thermomagnetic behavior typical of titanomagnetites. Type I and II behavior occurs throughout the hole, although type II behavior is most common below 330 mbsf, and there is no clear change in the inversion temperature or of the peak temperature of the

Table 3. Measurements of susceptibility at high temperature, Hole 896A.

Core, section, interval (cm)	Piece	Lithology	Unit	Depth (mbsf)	Bulk susceptibility ($\times 10^{-3}$ SI units)	J_0 (A/m)	Inclination (°)	Median destructive field (mT)	Peak 1 (°C)	Trough (°C)	Peak 2 (°C)	T_{max} (°C)	Type
148-896A-													
3R-1, 68	8	P	8	210.58	9.4	9.338	−7	17				658	II
6R-1, 93	9b	P	12	238.83	17.4	22.46	−19	15	300	360	440	670	Ia
7R-1, 38	7	P	13	247.78	2.2	3.462	0	40			630		
7R-1, 101	15	P	14	248.41	6.8	12.74	−10.5		305	365	470	600	Ia
8R-1, 29	7	P	14	257.39	9.1	11.4	−34		300	350	470	585	Ib
9R-2, 6	1	P	14	268.16	5.6	10.56	−7	28	280	375	420	595	Ia
10R-1, 70	8b	M	14	277.1	5.6	12.35	−3	25	290	385	430	585	Ia
14R-2, 118	16b	M	21	317.18	16.1	6.221	−4		295	355	400	540	Ia
14R-3, 65	11	M	21	318.15	10.4		−11		322	482	520	656	Ib
15R-1, 3	1	M	22	324.33		10.65	−21	12	300	360	420	580	Ia
16R-2, 50	1e	M	24	335.7	26.6	5.776	14	9	280	360		490	Ia
16R-2, 113	4b	M	24	336.33	17.3	6.645	−5	7	440	540		700	II
16R-3, 81	4a	M	24	337.51	19.6	4.459	−9	8	435	545		700	II
17R-2, 140	12b	P	27	346.4	22.2	7.33	0	9	320	468	521	560	II
18R-1, 102	9b	P	29	354.12	21.0	13.8	0	17	312	400	450	700	Ia
21R-1, 137	20	M	31	374.37	19.6	1.044	−5	8	310	380	410	550	II
22R-1, 45	5b	M	32	383.05	20.8	6.569	−37	14	310	380	450	600	Ia
23R-2, 82	7	M	36	394.42	18.6	0.785	−20	10	312	385	435	550	II
24R-2, 85	10	M	36	404.15	23.0	1.187	44	13	420	542		720	II
24R-2, 114	13	M	36	404.44	24.2	1.322	27	8	330	367	420	560	II
25R-1, 34	6	P	37	411.64	13.7	2.685	15	15	310	405	442	700	Ic
25R-2, 89	16	P	37	413.69	11.2	2.435	−31	15	305	400	430	605	Ia
27R-3, 43	5	P	47	433.83	17.1	2.306	−8	14	330	405	440	700	Ia
Mean									324	410	445	619	
SD									47	65	34	65	
Mean above 330 mbsf									299	379	446	610	
SD									12	43	39	42	
Mean between 330 and 360 mbsf									357	463	486	630	
SD									75	83	50	99	
Mean below 360 mbsf									328	408	432	623	
SD									38	56	14	72	

Notes: Peak 1 = temperature of the first peak; Trough = temperature of the trough between the two peaks; Peak 2 = temperature of the second peaks; and T_{max} = temperature at which the susceptibility drops to zero. Type is defined in the text. SD = 1 standard deviation.

product with depth. The absence of change in these temperatures, which are highly sensitive to the ratio of Fe to Ti and other cations, suggests that there is little change in the relative abundance of the cations, although the increase in the occurrence of type II behavior may be related to subtle changes in the stoichiometry of the iron oxides.

MAGNETIC MINERALOGY

The core recovered in Hole 896A can be separated into upper, middle, and lower sections that exhibit different magnetic properties. The first boundary, between the upper and middle sections (at about 330 mbsf), is marked by a distinct rise in susceptibility (Fig. 3). The second boundary, between the middle and lower sections (at about 360 mbsf), is based on a decrease in J_0, a higher scatter in the stable magnetic inclinations, and an increase in the maximum susceptibility recorded downhole. The MDF appears to decrease more gradually downhole. The upper section (above 330 mbsf) has high J_0 values (11.2 ± 4.2 A/m), high magnetic stability (MDF = 26.2 ± 11.8 mT), and low bulk susceptibilities (9.1 ± 4.0 × 10^{-3} SI units). The middle section (between 330 and 360 mbsf) is bounded at the top by the massive flow Unit 24. J_0 is high (8.0 ± 4.1 A/m), but magnetic stability (MDF) is low (11.6 ± 4.5 mT) and susceptibility is high (21.9 ± 4.2 × 10^{-3} SI units). The magnetic remanence is characterized by single stable magnetic components in both the upper and middle sections. The lower section (below 360 mbsf to the bottom of the hole at 469 mbsf) is bounded at the top by the first of a package of massive flows (Units 31–36). In this section J_0 is low (3.1 ± 2.4 A/m), MDF is low (10.7 ± 5.6 mT), and the susceptibility is high and variable (26.8 ± 11.0 × 10^{-3} SI units). The magnetic components show great circle trajectories, indicating overprinting, and the inclinations show a high degree of scatter.

The transitions between these sections (at 330 and 360 mbsf) do not correspond to the bulk change in petrology observed in the core; the change between plagioclase-olivine phyric basalt above to plagioclase-olivine-clinopyroxene phyric basalt below occurs at about 390 mbsf. There is, however, a distinct change in the TiO_2 content, and a more subtle change in Fe_2O_3, at a depth of about 345 mbsf (see Alt, Kinoshita, Stokking, et al., 1993). This geochemical change is also reflected in other elemental compositions, including SiO_2 and CaO.

The saturation remanence (J_{rs}) shows a variation downhole similar in form to that of Fe_2O_3. This parameter probably represents a good estimate of the amount of ferrous oxide in the basalt, and it varies by a factor of about 20%. This suggests that the actual concentration of the oxide phase does not contribute significantly to the variation in magnetization, which is much larger.

Another important control on the magnetic properties is the grain size. This property is difficult to measure directly, because the opaque grains in the fine-grained or microcrystalline groundmass are in general below optical resolution. We have attempted to quantify the effect of grain-size variation by estimating the average grain size from one property (MDF) assuming that the concentration and composition are invariant, and then using this to generate an estimate of the other properties, which can be compared with the actual measurements. This is similar to the approach adopted by O'Reilly et al. (1993), although they used more complex parameters, including a simultaneous estimate of the degree of maghematization and grain size. We do not think that this is appropriate for this data set because we have not measured the degree of maghematization and because this model is appropriate only for a narrow range of compositions. The grain size of the magnetites has been related to the hysteresis properties, particularly the coercive force, H_c (Heider et al., 1987). This relationship is not entirely suitable for titanomagnetites (see, e.g., fig. 7.9 in O'Reilly, 1984), but it does give an indication of the variation in grain size, though not any absolute values. Although we do not have direct measurements of the coercive force for samples from this hole, Furuta (1983) showed that there is a strong correlation

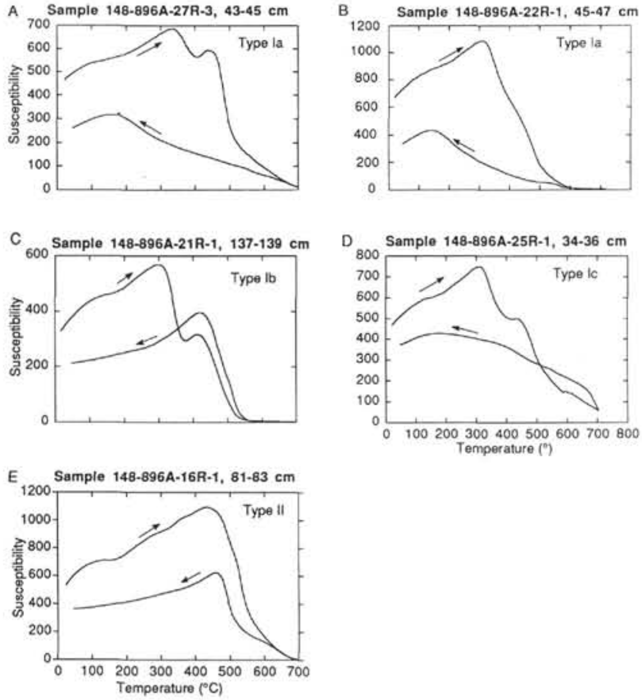

Figure 4. Bulk susceptibility vs. temperature. Heating and cooling runs are indicated by arrows. **A.** Type Ia irreversible thermomagnetic curve with well-defined first peak, trough, and second peak. The cooling curve shows a gradual slope, rising to a peak at about 200°C. **B.** Type Ia irreversible thermomagnetic curve with well-defined first peak, steep slope, first point of inflection (corresponding to the trough), shallower slope, second point of inflection (corresponding to the second peak), and steeper slope. The cooling curve shows a gradual slope, rising to a peak at about 200°C. **C.** Type Ib irreversible thermomagnetic curve. The cooling curve has a steep slope, with a peak at about 500°C. **D.** Type Ic irreversible thermomagnetic curve. The cooling curve rises between 600° and 700°C. **E.** Type II partially reversible thermomagnetic curve, reaching a single peak at about 450°C. The cooling curve also shows a peak at about 460°C, although with a lower susceptibility. Note that all curves have a bulge on their heating slopes between about 30° and 200°C, which is also visible on some of the cooling curves.

between H_c and MDF. We have used this correlation to estimate H_c from the MDF of samples from Hole 896A, and thus to estimate the grain size of samples (Fig. 5A). We can go further, and test to what extent J_0 and susceptibility can be explained by a simple variation in grain size. The variation of susceptibility with grain size has been discussed by O'Reilly (1984) for different compositions, including $x = 0.61$, which we have chosen to use. From this variation we can predict the variation in susceptibility (although not any absolute values). This estimate is shown in Figure 5B. The strong correlation between the estimated and measured values of susceptibility (Fig. 5D) suggests that a large part of the variability in this parameter is related to changes in grain size without any need to evoke significant variability in magnetic mineralogy or concentration of magnetic grains. This is supported by the correlation between susceptibility and the log of MDF (Fig. 5F), which from the model of O'Reilly et al. (1993) would be expected if the variation in the degree of maghematization and the concentration are insignificant.

We can also estimate J_0 assuming that the magnetization is similar to a thermo-remanent magnetization (TRM) (if the magnetic mineral is maghemite, this case is not likely; however, Thellier-Thellier experiments [S. Allerton, unpubl. data] suggest that the magnetization may mimic a TRM), using the parameters published by Dunlop

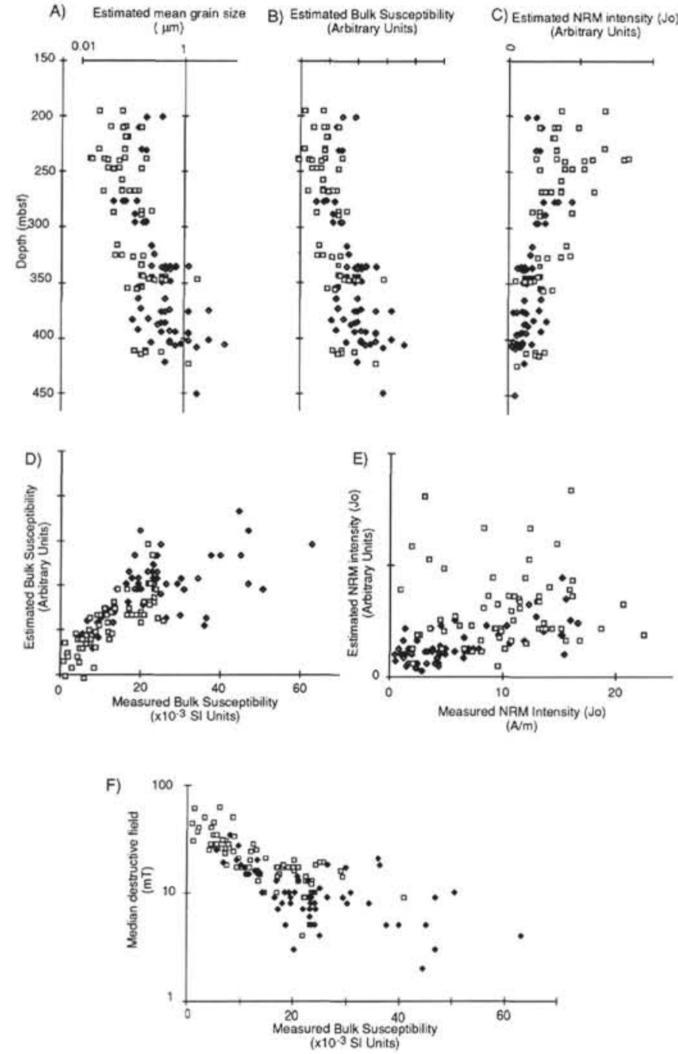

Figure 5. **A.** Estimate of the grain size of magnetic grains vs. depth. **B.** Bulk susceptibility estimated from grain size vs. depth. **C.** J_0 estimated from grain size vs. depth. **D.** Correlation of estimated and measured bulk susceptibility. **E.** Correlation of estimated and measured J_0. **F.** MDF plotted on a log scale vs. bulk susceptibility.

(1981). This estimate (Fig. 5C, E) can explain some of the general features of the curve—the high magnetization in the upper part of the hole and lower magnetization in the lower part. The estimate does predict some particularly high values of J_0 in the middle of the upper part of the hole that were not observed. Other factors will control J_0, particularly the degree of maghematization and the magnetization process (for example, thermal or chemical remanence), so it is perhaps not surprising that J_0 cannot be modeled by grain size alone.

Evidence for hematite from reversible thermomagnetic behavior in the 600° to 700°C range and from high values of H_{sat} from IRM acquisition are restricted largely to the thick massive flow Units 21, 24, and 36. These exhibit high levels of pervasive alteration, and hematite has been reported in thin section from Unit 36 (Alt, Kinoshita, Stokking, et al., 1993).

Furuta and Levi (1983) suggested that the largest control on magnetic properties in Hole 504B is lithologic, related to grain size, with high J_0 and low susceptibilities in pillow flows and low J_0 and high susceptibilities in massive flows. The results of this study indicate that within each of the sections identified in Hole 896A, the massive flows and pillow flows have slightly different properties, but that the differences in the properties of pillow flows and massive flows between the sections is greater than that between the types of flows in any individual section.

COMPARISON WITH HOLE 504B

The magnetic properties of the upper part of the extrusive sequence of Hole 504B have been described by Furuta and Levi (1983) (see Table 2). The first 39 m of the basement of Hole 504B, to the top of massive flow Unit 2D (313 mbsf), has many properties in common with the first 135 m of basement in Hole 896A (see Table 2). For example, J_0 in Hole 504B is 11.2 ± 5.0 A/m, compared to 11.2 ± 4.2 A/m in Hole 896A, and the bulk susceptibility in Hole 504B is 11.7 ± 5.8 × 10^{-3} SI units, compared to 13.8 ± 5.6 × 10^{-3} SI units in Hole 896A. The stable inclinations are also similar: −10.8° ± 6.0° in Hole 504B compared to −9.2° ± 10.5° in Hole 896A. Both of these values are close to the expected paleoinclination (−7°), suggesting that there has been little tilting of this part of the sequence. The base of these sequences is at 3773 ± 3 mbsl in Hole 504B and at 3796 ± 3 mbsl in Hole 896A (see Fig. 6). Comparison of the geochemistry of these two holes shows that they both show an increase in TiO_2 and a decrease in Al_2O_3 and in Cr at about this level. It does not necessarily follow that these upper extrusive rocks are from identical flows or volcanic sources, but it is likely that they are of a similar origin, post-dating the flow beneath.

Below 313 mbsf in Hole 504B, basement has properties similar to the lower section of Hole 896A (see Table 2). For example, in Hole 504B the bulk susceptibility is 27.7 ± 13.5 × 10^{-3} SI units, whereas it is 26.8 ± 11.0 × 10^{-3} SI units in Hole 896A. J_0 is 5.7 ± 5.3 A/m in Hole 504B and 3.1 ± 2.4 A/m in Hole 896A. The inclinations in Hole 504B below 313 mbsf are −23.7° ± 21.0°, which Furuta and Levi (1983) have related to a tilting of the extrusive rocks away from the axis.

IMPLICATIONS FOR THE EVOLUTION OF SITES 504 AND 896

The upper sections of Holes 504B and 896A have features that suggest that they were extruded slowly, a few kilometers away from the ridge axis, onto an approximately level, perhaps ponded, flow surface, and that the section below was extruded close to the axis.

The reasons for making this assertion can be summarized as follows:

1. The very fine grain sizes indicated by the magnetic stability may result from slow effusion, which allows rapid cooling.
2. If the apparently cyclical nature of the magnetic inclinations in the upper section results from secular variation, then extrusion occurred gradually over a few thousand years.
3. The inclinations of the upper sections of Holes 504B and 896A are very close to the stable reference inclination, suggesting that the upper section has not been tilted. In Hole 504B, the section below has been tilted, suggesting that these sections are separated by an unconformity.
4. Pervasive alteration is much more extensive in the lower part of the section (Alt, Kinoshita, Stokking, et al., 1993). This suggests that either the upper section was extruded after the main phase of hydrothermal circulation was over, or that the massive flow unit acted as an effective seal to hydrothermalism beneath. Pezard (1990) has emphasized the importance of Unit 2D in Hole 504B as a hydrological barrier, from various downhole logs and from packer and temperature measurements.
5. The base of the upper sections is at 3773 ± 3 mbsl in Hole 504B and at 3793 ± 3 mbsl in Hole 896A, so the upper sequence was built up on an approximately level top surface of a massive flow (Fig. 6). The apparent dip of this surface between the two holes is about 2°. The thickness of this flow unit is between 24.0 and 10.4 m in Hole 504B and between 9.1 and 3.6 m in Hole 896A, consistent with ponding of the flow.

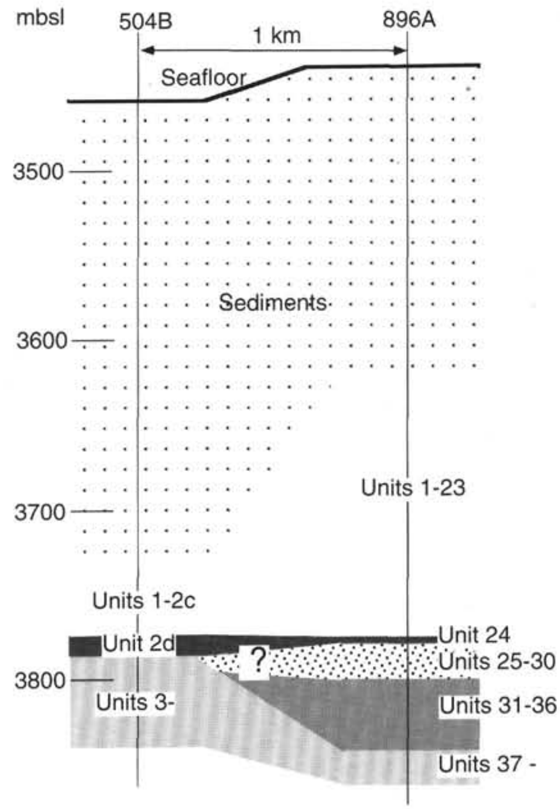

Figure 6. Cartoon illustrating the correlation between Hole 504B and Hole 896A based on magnetic properties.

CONCLUSIONS

The basement of Hole 896A can be divided into three sections on the basis of its magnetic properties (see Table 2 and Fig. 3). The upper section, to 330 mbsf, has relatively high J_0 and low susceptibility values. The middle section, between 330 and 360 mbsf, has a high J_0 and intermediate susceptibility values, and the lower section, below 360 mbsf, has low J_0 and high susceptibility values. The magnetic stability and susceptibility can be related to the size of the magnetic grains. The values of J_0 can be modeled by grain size in a broad sense, but in detail the effects of the maghematization and magnetization process probably also control the intensity of magnetization.

The magnetic properties of the basement of Hole 896A can be correlated with those of Hole 504B. The base of the upper section corresponds to the massive flow Unit 24 in Hole 896A and to the massive flow Unit 2D in Hole 504B. The apparent dip of this level between the two holes is about 2°. The upper section probably represents an off-axis lava pile with an irregular upper surface topography that was extruded over a relatively long period of time. The massive flow unit at its base apparently acted as an important barrier to hydrothermal fluids, focusing alteration beneath it.

These results have significant implications for the interpretation of magnetic field data from ridges. The uppermost layer of late extrusive rocks has a high magnetization and a highly variable thickness;

it may be an important contributor to variations in the magnetic signal at ridges. Thus, magnetic segmentation (Sempere, 1991) may result from the increased thickness of late extrusive rocks rather than from variations in the magnetization of the basalt sequence as a whole.

ACKNOWLEDGEMENTS

We would like to thank W. O'Reilly, S. Beske-Diehl, and Carl Richter for providing thoughtful and constructive reviews of this paper. Particular thanks go to M. Halstedt for her advice and assistance on the *JOIDES Resolution*.

REFERENCES

Ade-Hall, J.M., and Johnson, H.P., 1976. Paleomagnetism of basalts, Leg 34. *In* Yeats, R.S., Hart, S.R., et al., *Init. Repts. DSDP,* 34: Washington (U.S. Govt. Printing Office), 513–532.

Allerton, S., Pariso, J.E., Stokking, L.B., and McClelland, E., 1995. Origin of the natural remanent magnetism of sheeted dikes in Hole 504B cored during Legs 137 and 140. *In* Erzinger, J., Becker, K., Dick, H.J.B., and Stokking, L.B. (Eds.), *Proc. ODP, Sci. Results,* 137/140: College Station, TX (Ocean Drilling Program), 263–270.

Alt, J.C., Kinoshita, H., Stokking, L.B., et al., 1993. *Proc. ODP, Init. Repts.,* 148: College Station, TX (Ocean Drilling Program).

Banerjee, S.K., 1980. Magnetism of the oceanic crust: evidence from ophiolite complexes. *J. Geophys. Res.,* 85:3556–3566.

Cande, S.C., and Kent, D.V., 1992. A new geomagnetic polarity time scale for the Late Cretaceous and Cenozoic. *J. Geophys. Res.,* 97:13917–13951.

Donovan, J.B., and O'Reilly, W., 1983, Magnetic properties of basalts from Hole 504B, Deep Sea Drilling Project Leg 69. *In* Cann, J.R., Langseth, M.G., Honnorez, J., Von Herzen, R.P., White, S.M., et al., *Init. Repts. DSDP,* 69: Washington (U.S. Govt. Printing Office), 721–726.

Dunlop, D.J., 1981. The rock magnetism of fine particles. *Phys. Earth Planet. Inter.,* 26:1–26.

Furuta, T., 1983. Magnetic properties of basalt samples from Holes 504B and 505B on the Costa Rica Rift, Deep Sea Drilling Project Legs 69 and 70. *In* Cann, J.R., Langseth, M.G., Honnorez, J., Von Herzen, R.P., White, S.M., et al., *Init. Repts. DSDP,* 69: Washington (U.S. Govt. Printing Office), 711–720.

Furuta, T., and Levi, S., 1983. Basement paleomagnetism of Hole 504B. *In* Cann, J.R., Langseth, M.G., Honnorez, J., Von Herzen, R.P., White, S.M., et al., *Init. Repts. DSDP,* 69: Washington (U.S. Govt. Printing Office), 697–703.

Heider, F., Dunlop, D.J., and Sugiura, N., 1987. Magnetic properties of hydrothermally recrystallized magnetite crystals. *Science,* 236:1287–1290.

Hobart, M.A., Langseth, M.G., and Anderson, R.N., 1985. A geothermal and geophysical survey on the south flank of the Costa Rica Rift: Sites 504 and 505. *In* Anderson, R.N., Honnorez, J., et al., *Init. Repts. DSDP,* 83: Washington (U.S. Govt. Printing Office), 379–404.

Johnson, H.P., 1978. Paleomagnetism of igneous rock samples—DSDP Leg 45. *In* Melson, W.G., Rabinowitz, P.D., et al., *Init. Repts. DSDP,* 45: Washington (U.S. Govt. Printing Office), 387–396.

Kirschvink, J.L., 1980. The least-squares line and plane and analysis of palaeomagnetic data. *Geophys. J. R. Astron. Soc.,* 62:699–718.

LaBrecque, J.L., Kent, D.V., and Cande, S.C., 1977. Revised magnetic polarity time scale for Late Cretaceous and Cenozoic time. *Geology,* 5:330–335.

Langseth, M.G., Mottl, M.J., Hobart, M.A., and Fisher, A., 1988. The distribution of geothermal and geochemical gradients near Site 501/504: implications for hydrothermal circulation in the oceanic crust. *In* Becker, K., Sakai, H., et al., *Proc. ODP, Init. Repts.,* 111: College Station, TX (Ocean Drilling Program), 23–32.

Lowrie, W., and Kent, D.V., 1978. Characteristics of VRM in ocean basalts. *J. Geophys.,* 44:297–315.

O'Reilly, W., 1984. *Rock and Mineral Magnetism:* New York (Chapman and Hall).

O'Reilly, W., Brown, K., Styles, P., and Bloxam, T.W., 1993. A detailed geochemical and rock magnetic study of dredged basalt from the Sheba Ridge, Gulf of Aden. *Mar. Geophys. Res.,* 15:101–119.

Ozdemir, O., and O'Reilly, W., 1981. Laboratory synthesis of aluminum-substituted titanomaghemites and their characteristic properties. *J. Geophys.,* 49:93–100.

Pariso, J.E., and Johnson, H.P., 1991. Alteration processes at Deep Sea Drilling Project/Ocean Drilling Program Hole 504B at the Costa Rica Rift: implications for magnetization of oceanic crust. *J. Geophys. Res.,* 96: 11703–11722.

Pechersky, D.M., Tikhonov, L.V., and Pertsev, N.N., 1983. Magnetic properties of basalts, Deep Sea Drilling Project Legs 69 and 70. *In* Cann, J.R., Langseth, M.G., Honnorez, J., Von Herzen, R.P., White, S.M., et al., *Init. Repts. DSDP,* 69: Washington (U.S. Govt. Printing Office), 705–710.

Pezard, P.A., 1990. Electrical properties of mid-ocean ridge basalt and implications for the structure of the upper oceanic crust in Hole 504B. *J. Geophys. Res.,* 95:9237–9264.

Sempere, J.-C., 1991. High-magnetization zones near spreading center discontinuities. *Earth Planet. Sci. Lett.,* 107:389–405.

Smith, G.M., and Banerjee, S.K., 1986. Magnetic structure of the upper kilometer of the marine crust at Deep Sea Drilling Project Hole 504B, Eastern Pacific Ocean. *J. Geophys. Res.,* 91:10337–10354.

Vine, F.J., and Moores, E.M., 1972. A model for the gross structure, petrology, and magnetic properties of oceanic crust. *Mem.—Geol. Soc. Am.,* 132:195–205.

Date of initial receipt: 15 August 1994
Date of acceptance: 24 February 1995
Ms 148SR-129